Highly photodegradation of organic dye pollutant RhB using TiO2-modified reduced graphene oxide

Rahmat Hidayat
Universitas Sebelas Maret
Sayekti Wahyuningsih
Universitas Sebelas Maret
Ganjar Fadillah (ganjar.fadillah@uii.ac.id)
Universitas Islam Indonesia
Ari Handono Ramelan
Universitas Sebelas Maret

Research Article

Keywords: TiO2, reduced graphene oxide, rGO-TiO2, photocatalytic degradation, Rhodamine-B

Posted Date: June 25th, 2021

DOI: https://doi.org/10.21203/rs.3.rs-638640/v1

Abstract

TiO_2-modified reduced graphene oxide (TiO_2-rGO) has been studied in one-process step synthesis via the hydrothermal method. In this study, the various concentrations of rGO were investigated and characterized by fourier transform infrared (FTIR), x-ray diffraction (XRD), scanning electron microscope (SEM), surface area analyzer (SAA), thermogravimetric analysis/differential thermal analysis (TGA/DTA), and spectroscopy UV-Vis. In addition, the photodegradation of rhodamine-B was studied by a batch system under visible light irradiation at wavelength 554 nm. The optimum experimental results showed that the presence of rGO in TiO_2 nanostructures could improve the specific surface area until 248.58 $m^2 g^{-1}$ and enhanced the photodegradation efficiency until 70.66% under visible light irradiation. The photocatalyst stability was evaluated for five cycles experiment and the performance have reduced 6.58% efficiency.

1. Introduction

Water contamination becomes severe problem in the world because of its importance for human life. The lower water quality contains dangerous substance such as carcinogenic dyes, heavy metals, pharmaceutical waste [1]. Dyes contaminant comes from textile industry that contains soluble mineral salts, aromatic and halogen compound mixture [2]. The dye waste can be treated by ionic exchange precipitation, evaporation, reverse osmosis, ultrafiltration, and solvent extraction [3]. Photodegradation technique is more interesting because of simple relatively, good stability, no expensive [4] and carbonaceous product [5]. TiO_2 material is attractive for photocatalysis because it has bandgap energy of ~ 3.0-3.2 eV that can be active in wavelength of ~ 390 nm and free-electron movement with shorter line distance averages [6]. However, TiO_2 only work optimally in the ultraviolet range and electron-hole recombination that causes less optimal degradation efficiency [7, 8].

The performance of TiO_2 depends on size, composition, crystal phase, crystallinity, specific surface area and morphology [9, 10]. The higher specific surface area impacts on enhancement of substrate and photocatalyst interaction so that photodegradation effectiveness optimally increases. The sub-micron light scattered impacts the enhancement of the photon movement pathway's length in photoanode, then it can improve light absorption and efficiency [11]. Photocatalytic activity of TiO_2 can be improved again with composite or hybrid formation by metal or non-metal. Graphene-based composite with semiconductor has been reported as photocatalyst material such as TiO_2/graphene, ZnO/graphene, Ta_2O_5/graphene [12], Cu_2O/graphene [13] and CdS/graphene [14].

The TiO_2 modification with graphene-like (reduced graphene oxide) can improve the photocatalytic activity of semiconductor. The reduced graphene oxide (rGO) existence causes the redshift of light absorption and slower recombination. Besides that, enhancement of photocatalytic activity occurs because the rGO decorated TiO_2 (rGO-TiO_2) do strong interaction that initiates the electron injection and electron transport from TiO_2 to rGO so that inhibits electron-hole recombination [15]. In this work, TiO_2 will

be synthesized with rGO simultaneous by a one-pot process using the hydrothermal method for improving photocatalytic properties by using rhodamine-B (RhB) as a dye for photocatalytic degradation experiment under visible light irradiation.

2. Experimental Methods

2.1. Materials

Titanium (IV) tetraisopropoxide (TTIP) (≥ 99%) and dihydrate oxalic acid (≥ 99%) were obtained from Sigma Aldrich. NaOH (≥ 97%) and hydrochloric acid (37 %) were used from Merck. Deionized (DI) water was obtained from Water purification system Millipore. Graphene oxide (GO) powder was obtained from synthesize of graphite flake.

2.2. Procedure

The TTIP was reacted with 0.362 M oxalic acid in a ratio of 1 : 2.2 mol. After that, GO powder was added by 2%, 4%, and 10% (w/w). Then, 8 g of NaOH was mixed to the mixture slowly with a constant stirring until all of NaOH pellets were dissolved and formed gel. Gel was further treated by hydrothermal process at a temperature of 200 ^{o}C during 24 hours. The hydrogel was cooled and washed with 1 liters of 0.1 M HCl followed with 1 liters deionized water until reach pH of 8. The precipitate was dried by freeze drying technique until obtained powder, then heated at 100 ^{o}C for 12 hours. After that, the powder was heated at 300 ^{o}C for 3 hours to obtain rGO-TiO_2 powder.

2.3. Characterization

Spectrophotometer UV-Vis Perkin-Elmer Lambda 25 was used to observe absorption spectra in ultraviolet and visible wavelength. The functional groups were performed by Spectrophotometer Fourier Transform Infra-Red (FTIR) IR Prestige-21. The X-ray diffraction pattern was recorded with Powder XRD Rigaku Miniflex 600 Benchtop using CuKα radiation (λ = 0.15406 nm). Scanning Electron Microscopy (SEM) Vega 3 Tescan was used for morphology characterization. The surface area and pore distribution was measured by Surface Area & Pore Analyzer (SAA) Quantachrome Nova 1200e. Thermal analysis of decomposition material process was performed by Thermogravimetric Analysis/Differential Thermal Analysis (TG/DTA) Linseis STA PT-1600.

3. Results

TiO_2 decorated rGO (rGO-TiO_2) have been synthesized by a base hydrothermal method in a one-pot process. TiO_2 was obtained from titanium oxalate precursors that ti-oxalate was obtained from the reaction of TTIP with oxalic acid refer to reference [9]. Figure 1 shows that synthesized TiO_2 material has a broadening peak indicating an amorphous crystal structure where the results were not the same as shown by Huang et al. (2016) [9] and Zhao et al. (2017) [10], which has high and narrow peaks. The appearance of dominant peaks is also seen in only two peaks, namely at $2\theta = 25.33^{o}$ and 48.36^{o}. The

25.33^{o} peak indicates the anatase [d_{101}] of the TiO_2 refer to [10], while the 48.36^{o} peak indicates the anatase [d_{004}] [9, 15]. The other anatase crystal planes (d) of [103], [200], [105], [211], [116], [220], [215] and [303] only appear in small peaks, which indicate that the TiO_2 crystals have not yet grown perfectly so that the diffractogram pattern shows a low of crystallinity (peak broadening). The anatase phase is the metastable phase of TiO_2 before it becomes rutile, where the anatase phase is thermodynamically stable at smaller particle sizes (< 11 nm) while rutile is stable at larger sizes (> 35 nm) [16].

The Diffractogram of TiO_2 - rGO hybrid material shows different patterns for the addition of 2%, 4% and 10% GO. The diffraction pattern of TiO_2 - rGO 2 shows two peaks at 2θ = 25.30^{o} and 48.36^{o} correspond to [101] and [004] of anatase phase TiO_2 material. Then, the peaks at 2θ = 10.76^{o} and 28.42^{o}, respectively indicate peaks [001] of GO and [002] of rGO [8]. GO diffraction peaks indicates that the presence of TiO_2 impacts the GO formation where at the reduction temperature of 300 ^{o}C without TiO_2, rGO has formed perfectly as in Fig. 1. TiO_2 material can increase the thermal resistance of GO so that at the same temperature, GOs are not converted to rGO. The diffractogram of TiO_2 - rGO 4 and TiO_2 - rGO 10 is different from TiO_2 - rGO 2 diffraction patterns. The appearance of GO dominant peak at 2θ = 12.94^{o} makes anatase TiO_2 peaks smaller, while rGO [002] appears at 2θ = 28.95^{o}. The peak of TiO_2 [101] decreases with increasing GO addition that covers the existence of other peaks and it can also be known that TiO_2 influences the formation of rGO, but also TiO_2 growth is affected by GO, so the growth of TiO_2 crystals is inhibited. Because the presence of GO is increasing and the amount of TiO_2 is relatively fixed so GO cannot interact to TiO_2 uniformly. At the same reduction temperature, more GO are converted to rGO for the addition of GO 2%.

The X-ray diffraction results are supported by FTIR characterization data that is shown in Fig. 2. The spectra of TiO_2 have absorption at 468 cm^{-1} and 908 cm^{-1} wavenumbers which indicate the existence of stretching and binding vibrations of Ti-O-Ti and Ti-O [16, 17]. Then, the absorption at wave numbers of 1626 cm^{-1} and 3383 cm^{-1} show the stretching vibration of the hydroxyl functional group (OH) which is derived from the absorption of H_2O molecules on the surface [18, 19]. Modification of TiO_2 with rGO is known from the appearance in the FTIR spectra of TiO_2 addition of 2, 4 and 10% GO. The three spectra showed relatively similar patterns of around 500 cm^{-1} as Ti-O-Ti and Ti-O-C vibration [20], absorption around 3400 cm^{-1} shows O-H vibrations. The bonding due to interactions between TiO_2 and rGO is characterized by new absorption band that appears at around 1000 cm^{-1} as the interaction of TiO_2 with C atoms from rGO [19, 21].

The broadening absorption at the wavenumber of 3400 cm^{-1} indicates the existence of the remaining O-H functional groups of irreducible rGO, which is useful as a site of interaction between rGO and TiO_2 [19]. Absorption around the wavenumber of 1600 cm^{-1} in the modified material spectra indicates the existence of vibrations from Ti-O-C bonds [22]. The results of X-ray diffraction characterization and FTIR spectrophotometry show that there is an interaction between TiO_2 and rGO.

SEM imaging obtained the micrograph that is shown in Fig. 3. Figure 3 (a) shows that it has an agglomerated shape so that it appears micro-sized agglomeration of TiO_2. Whereas the modification with 10% GO, Fig. 3 (b) shows that the graphene sheets (rGO) have micro-scale wrinkled layers which TiO_2 grows on its surface. The growth TiO_2 has a different morphology when growing alone (without rGO). TiO_2 is not agglomerated but instead shaped a nanometer size rod-like. It shows that rGO is used as an anchor agent for TiO_2 preventing agglomeration [19].

Surface area and pore analyzer characterization (Fig. 4) shows that materials of TiO_2, TiO_2 - rGO 2, TiO_2 - rGO 4 and TiO_2 - rGO 10 have relatively similar curve patterns that all curves based on the IUPAC classification have a type IV adsorption - desorption pattern [23] with hysteresis loops H_2 [15, 24]. According to Lv et al. (2017), if the hysteresis area of the loops is increasing, become less mesoporous.

Table 1
Surface area specific and averages pore size of TiO_2, TiO_2 - rGO 2, TiO_2 - rGO 4 and TiO_2 - rGO 10.

Material	BET Surface area (m^2/g)	Averages pore size (nm)
TiO_2	231.58	4.66
TiO_2 - rGO 2	216.35	5.98
TiO_2 - rGO 4	242.16	5.70
TiO_2 - rGO 10	248.58	6.36

In this study, the higher GO addition making the hysteresis area loops increase, then the mesoporous site increases. The BET active surface area from TiO_2 material is 231.58 m^2/ g (Table 1). The higher the active surface area, can improve the increasing ability to interact with reactants. The higher GO addition obtains a more considerable surface area value as well. Increasing surface area can also be caused by reduced aggregation of TiO_2 [25]. The decrease in aggregation due to rGO as an anchor agent is following SEM data in Fig. 3.

The maximum pore size distribution is shifting as more GO are added which is caused by a decrease in the aggregation of TiO_2 [24]. The pattern of broadening the pore size distribution (Fig. 5) also indicates the presence of mesoporous sites in the material that is by the adsorption-desorption data isothermal.

The bandgap energy indicates the minimum energy to excite electrons from the valence band to the conduction band for initiating catalysis reaction which the decrease in the bandgap shows the photocatalyst ability to work in visible light increases [18].

The bandgap energy measurement shows that TiO_2, TiO_2 - rGO 2, TiO_2 - rGO 4 and TiO_2 - rGO 10 materials have Eg values of respectively 3.01, 2.85, 2.83 and 2.82 eV. The Eg indicates that there has been a redshift (in the direction of visible light), as shown in Fig. 6. Testing of photodegradation performance of material modified against RhB was performed using the UV-Vis spectrophotometry method at a maximum λ of 554 nm. Measurements were performed in the range of 240 minutes by taking every 30 minutes. The initial 30 minutes measurement was performed with the lamp not turned on to achieve adsorption-desorption equilibrium [10, 20].

The tungsten lamp (300 W) was used as a source of visible light. Modification of TiO_2 with rGO can improve photodegradation performance where the percentage of degradation reached 26.49%, 29.30% and 34.32% for 2%, 4% and 10% GO addition. The increase in the percentage of RhB degradation is due to several things, such as increased active surface area and more visible light absorption [18].

Table 2
Percentage of photodegradation under visible and UV light irradiation.

Material	**% Degradation [a]**	
	Visible	**UV**
TiO_2	20.11	71.98
TiO_2-rGO 2	26.49	79.39
TiO_2-rGO 4	29.30	81.66
TiO_2-rGO 10	34.32	86.81
[a]: time of 240 minutes		
The electron transport in TiO_2-rGO causes the activation energy of electron excitation to decreases with Ti-O-C interaction, so the number of electron-holes photogenerated is increasing. Then, the excited electron does not directly recombine with the hole because of the presence of rGO that the electron will be transferred to the surface of rGO which has electronic conductivity properties.		

The photodegradation performance of the modified material was also carried out under UV irradiation, shown in Fig. 7 (b). The degradation percentage of the modified material also increases to 86.81% for the addition of 10% GO (Table 2). This enhancement shows that rGO can impact an increase of TiO_2 photodegradation activity.

The stability of photodegradation activity is shown in the graph in Fig. 8. Figure 8 shows that the photocatalyst is still working well after being used for five cycles, as evidenced by an insignificant decrease. The TiO_2-rGO 10 material even shows only a decrease of 6.58% after using five cycles. The ability of photocatalyst activity and good stability shows that modification with rGO can improve the

photocatalytic properties of TiO_2 where both materials work together to produce a good photodegradation performance [26] [27].

4. Conclusions

The characterization of FTIR and XRD showed Ti-O-C interaction; then it supported with morphology appearance. SEM showed that TiO_2 grows on rGO surface so the modification of TiO_2 with rGO in one-process synthesis has been done by the hydrothermal method. The TiO_2-rGO interaction reduces bandgap energy from 3.0 eV to 2.8 eV that indicates redshift (visible light). The photocatalytic performance had been evaluated toward RhB, which was known to improve about 70.66% from 20.11–34.32% under visible light irradiation and 71.98–86.81% (above 20%) under ultraviolet light irradiation. TiO_2-rGO has good stability in five cycles tests; the photocatalytic performance only decreased 6.58%, so photocatalytic activity of TiO_2 toward RhB increases with rGO modification.

References

1. N. Raghavan, S. Thangavel, G. Venugopal, Enhanced Photocatalytic Degradation of Methylene Blue by Reduced Graphene-Oxide/Titanium Dioxide/Zinc Oxide Ternary Nanocomposites. Mater. Sci. Semicond. Process. **30**, 321–329 (2015). https://doi.org/10.1016/j.mssp.2014.09.019
2. P. Nuengmatcha, S. Chanthai, R. Mahachai, W.C. Oh, Sonocatalytic Performance of ZnO/Graphene/TiO2 Nanocomposite for Degradation of Dye Pollutants (Methylene Blue, Texbrite BAC-L, Texbrite BBU-L and Texbrite NFW-L) under Ultrasonic Irradiation, Dyes and Pigments 134 (2016) 487–497. https://doi.org/10.1016/j.dyepig.2016.08.006.
3. P.V.A. Padmanabhan, K.P. Sreekumar, T.K. Thiyagarajan, R.U. Satpute, K. Bhanumurthy, P. Sengupta, G.K. Dey, K.G.K. Warrier, Nano-crystalline titanium dioxide formed by reactive plasma synthesis. Vacuum **80**, 1252–1255 (2006). https://doi.org/10.1016/j.vacuum.2006.01.054
4. M. Anas, D.S. Han, K. Mahmoud, H. Park, A. Abdel-Wahab, Photocatalytic degradation of organic dye using titanium dioxide modified with metal and non-metal deposition. Mater. Sci. Semicond. Process. **41**, 209–218 (2016). https://doi.org/10.1016/j.mssp.2015.08.041
5. K. Rajeshwar, J.G. Ibanez, G.M. Swain, Electrochemistry and the Environment. J. Appl. Electrochem. **24**, 1077–1091 (1994). https://doi.org/10.1007/BF00241305
6. B. Tang, H. Chen, H. Peng, Z. Wang, W. Huang, Graphene Modified TiO2 Composite Photocatalysts: Mechanism, Progress and Perspective, Nanomater. 8 (2018) 105. https://doi.org/10.3390/nano8020105.
7. X. Zhang, J. Qin, Y. Xue, P. Yu, B. Zhang, L. Wang, R. Liu, Effect of Aspect Ratio and Surface Defects on the Photocatalytic Activity of ZnO Nanorods. Sci. Rep. **4**, 1–8 (2014). https://doi.org/10.1038/srep04596
8. Y. Wang, X. Wang, M. Zhang, L. Fang, L. Jin, J. Gao, Y. Zhang, B. Yang, G. He, Z. Zun, TiO2 Nanorod Array Film Decorated with rGO Nanosheets for Enhancing Photocatalytic and Photoelectrochemical

Properties, J. Alloy. Compd. 770 (2019) 243–251. https://doi.org/10.1016/j.jallcom.2018.08.098.

9. X. Huang, L. Meng, M. Du, Y. Li, TiO2 Nanorods: Hydrothermal Fabrication and Photocatalytic Activities, J. Mater. Sci.: Mater. Electron.. 27 (2016) 7222–7226. https://doi.org/10.1007/s10854-016-4687-y.
10. J. Zhao, W. Li, X. Li, X. Zhang, Low Temperature Synthesis of Water Dispersible F-doped TiO2 Nanorods with Enhanced Photocatalytic Activity, RSC Adv. 7 (2017) 21547–21555. https://doi.org/10.1039/C7RA00850C.
11. M. Marandi, S. Bayat, M.N.S. Sabet, Hydrothermal Growth of a Composite TiO2 Hollow Spheres/TiO2 Nanorods Powder and Its Application in High Performance Dye-Sensitized Solar Cells, J. Electroanal. Chem. 833 (2019) 143–150. https://doi.org/10.1016/j.jelechem.2018.11.023.
12. H. Sun, S. Liu, S. Liu, S. Wang, A Comparative Study of Reduced Graphene Oxide Modified TiO2, ZnO and Ta2O5 in Visible Light Photocatalytic/Photochemical Oxidation of Methylene Blue, Appl. Catal. B: Environ. 146 (2014) 162–168. https://doi.org/10.1016/j.apcatb.2013.03.027.
13. L. Sun, G. Wang, R. Hao, D. Han, S. Cao, Solvothermal Fabrication and Enhanced Visible Light Photocatalytic Activity of Cu2O-Reduced Graphene Oxide Composite Microspheres for Photodegradation of Rhodamine B, Appl. Surf. Sci. 358 (2015) 91–99. https://doi.org/10.1016/j.apsusc.2015.08.128.
14. Q. Li, X. Li, S. Wageh, A.A. Al-Ghamdi, J.G. Yu, CdS/Graphene Nanocomposite Photocatalysts. Adv. Energ. Mater. **5**, 1–28 (2015). https://doi.org/10.1002/aenm.201500010
15. K. Lv, S. Fang, L. Si, Y. Xia, W. Ho, M. Li, Fabrication of TiO2 Nanorod Assembly Grafted rGO (rGO@TiO2-NR) Hybridized Flake-like Photocatalyst, Appl. Surf. Sci. 391 (2017) 218–227. https://doi.org/10.1016/j.apsusc.2016.03.195.
16. Z. Dargahi, H. Asgharzadeh, H. Maleki-Ghaleh, Synthesis of Mo-Doped TiO2/Reduced Graphene Oxide Nanocomposite for Photoelectrocatalytic Applications, Ceram. Int. 44 (2018) 13015–13023. https://doi.org/10.1016/j.ceramint.2018.04.120.
17. M. Darvishi, M. Jamali-Paghaleh, F. Jamali-Paghaleh, J. Seyed-Yazdi, Two methods for microwave irradiation synthesis of TiO2-ZnO-graphene ternary hybrids with enhanced photocatalytic activity, Mater. Res. Express. 4 (2017) 016501. https://doi.org/10.1088/2053-1591/aa52cf.
18. B. Singaram, J. Jeyaram, R. Rajendran, P. Arumugam, K. Varadharajan, Visible Light Photocatalytic Activity of Tungsten and Fluorine Codoped TiO2 Nanoparticle for an Efficient Dye Degradation, Ionics 25 (2019) 773–784. https://doi.org/10.1007/s11581-018-2628-x.
19. S.V. Nipane, S. Lee, G.S. Gokavi, A.N. Kadam, In Situ One Pot Synthesis of Nanoscale TiO2-Anchored Reduced Graphene Oxide (RGO) for Improved Photodegradation Of 5-Fluorouracil Drug, J. Mater. Sci.: Mater. Electron. 29 (2018) 16553–16554. https://doi.org/10.1007/s10854-018-9749-x.
20. Y.P. Putra, S. Wahyuningsih, A.H. Ramelan, R. Hidayat, Preparation of Fe2O3/ TiO2/Graphene Oxide Composite as Visible Light-Driven Photocatalytic in Degradation of Rhodamine B Dyes, Mater. Res. Express 6 (2019) 126207. https://doi.org/10.1088/2053-1591/ab56bc.

21. L. Tan, W. Ong, S. Chai, A.R. Mohamed, Reduced Graphene Oxide-TiO2 Nanocomposite as a Promising Visible-Light-Active Photocatalyst for The Conversion of Carbon Dioxide, Nanoscale Res. Lett. 8 (2013) 465. https://doi.org/10.1186/1556-276X-8-465.
22. H. Yan, T. Zhao, X. Li, C. Hun, Synthesis of Cu-doped Nano-TiO2 by Detonation Method, Ceram. Int. 41 (2015) 14204–14211. https://doi.org/10.1016/j.ceramint.2015.07.046.
23. A. Chakraborty, B. Sun, An Adsorption Isotherm Equation for Multi-types Adsorption with Thermodynamic Correctness. Appl. Therm. Eng. **72**, 190–199 (2014). https://doi.org/10.1016/j.applthermaleng.2014.04.024
24. W. Yu, X. Liu, L. Pan, J. Li, J. Liu, J. Zhang, P. Li, C. Chen, Z. Sun, Enhanced Visible Light Photocatalytic Degradation of Methylene Blue by F-Doped TiO2, Appl. Surf. Sci. 319 (2014) 107–112. https://doi.org/10.1016/j.apsusc.2014.07.038.
25. J.H. Pan, Z.Y. Cai, Y. Yu, X.S. Zhao, Controllable Synthesis of Mesoporous F-TiO2 Spheres for Effective Photocatalysis, J. Mater. Chem. 21 (2011) 11430–11438. https://doi.org/10.1039/C1JM11326G.
26. G. Fadillah, W.P. Wicaksono, I. Fatimah, T.A. Saleh, A sensitive electrochemical sensor based on functionalized graphene oxide/ SnO2 for the determination of eugenol, Microc. J. 159 (2020) 105353. https://doi.org/10.1016/j.microc.2020.105353.
27. G. Fadillah, T.A. Saleh, S. Wahyuningsih, E.N.K. Putri, S. Febrianastuti, Electrochemical removal of methylene blue using alginate-modified graphene adsorbents. Chem. Eng. J. **378**, 122140 (2019). https://doi.org/10.1016/j.cej.2019.122140

Figures

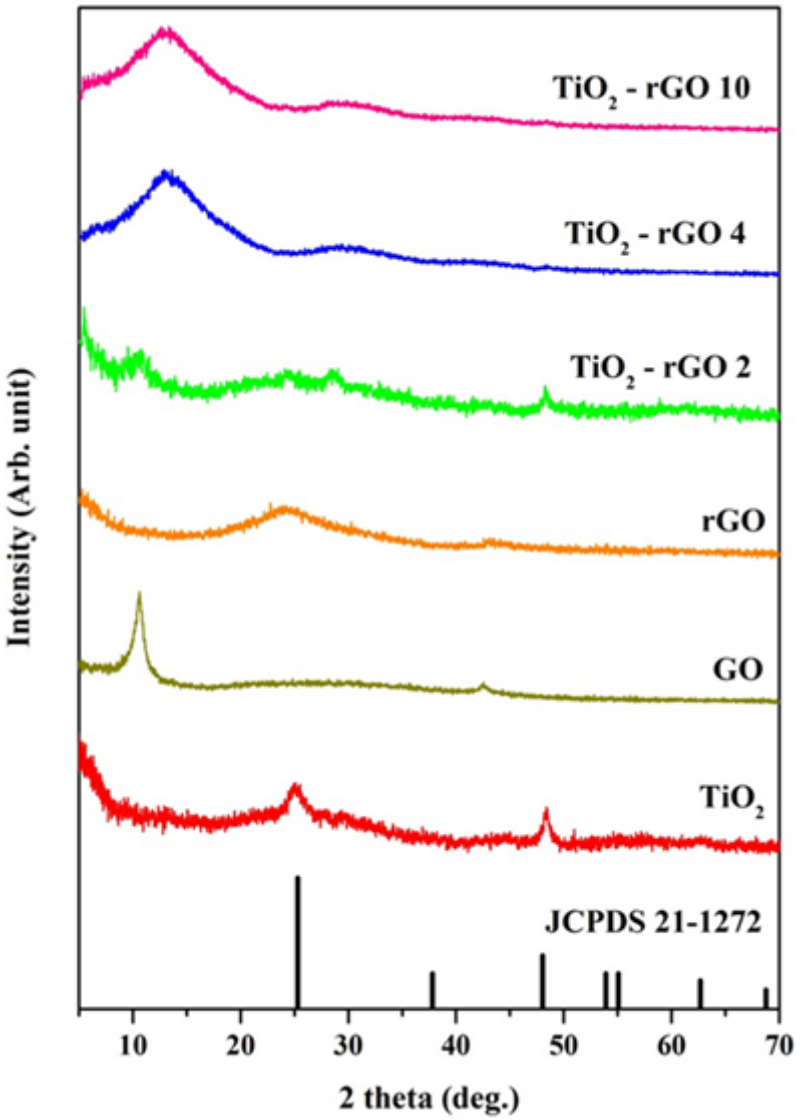

Figure 1

X-ray Diffractogram of modified material rGO-TiO compare with TiO2 standard, TiO2 (without rGO) and rGO.

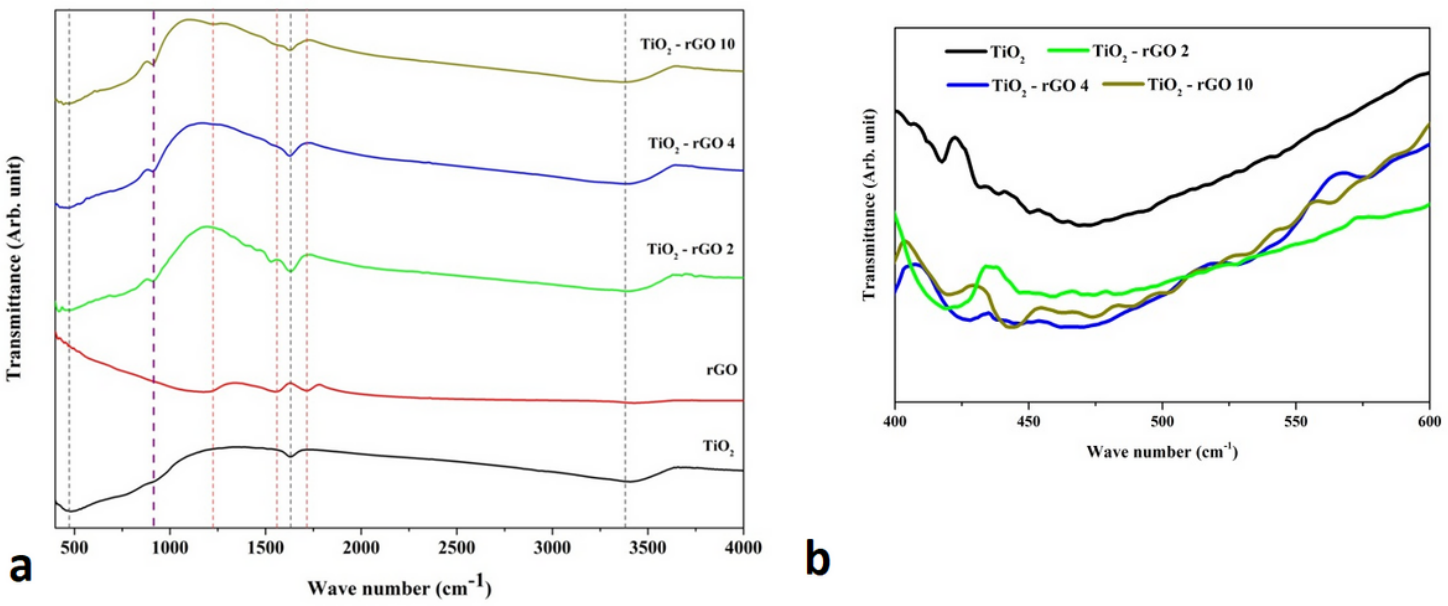

Figure 2

Comparison of modified material FTIR spectra with TiO2 and rGO at wavenumber of (a) 400 - 4000 cm-1 and (b) 400 - 600 cm-1.

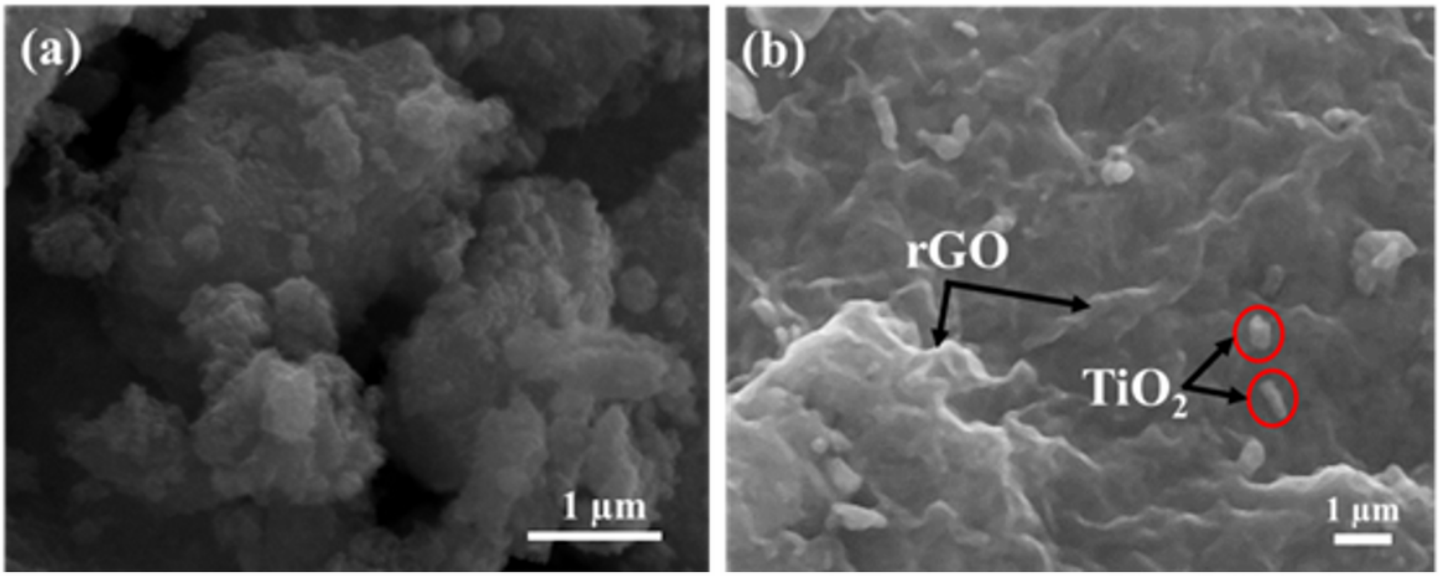

Figure 3

SEM Micrograph of (a) TiO2 and (b) TiO2- rGO 10.

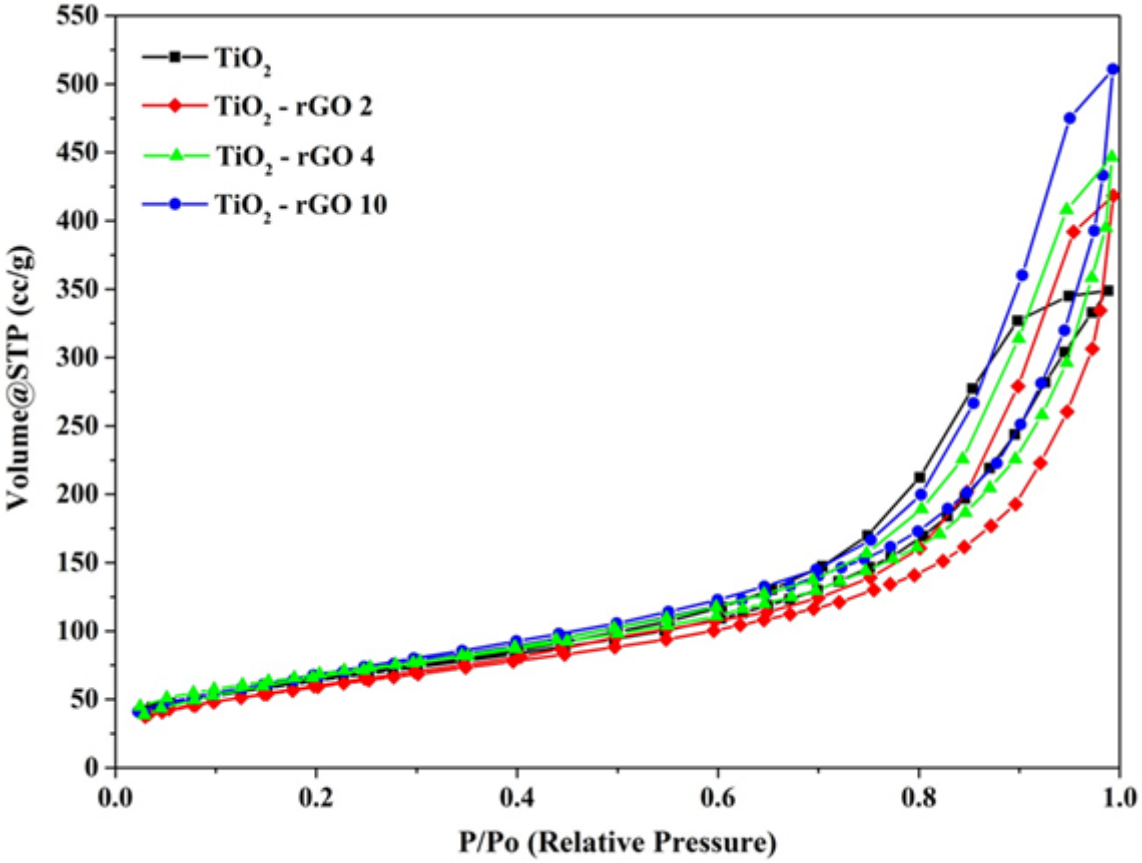

Figure 4

Graph of N2 adsorption-desorption isotherm of TiO2, TiO2 - rGO 2, TiO2 - rGO 4 and TiO2 - rGO 10.

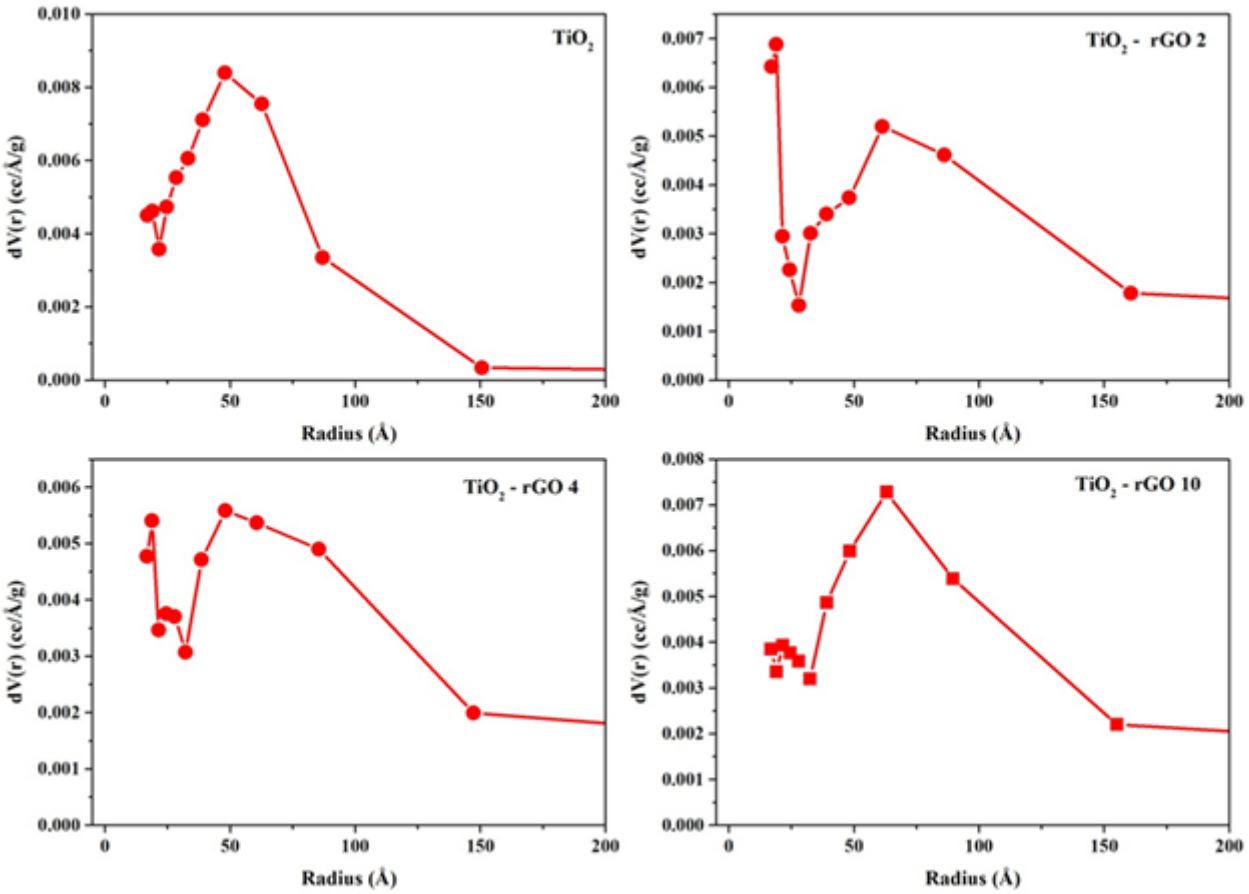

Figure 5

Pore size distribution of TiO2, TiO2 - rGO 2, TiO2 - rGO 4 and TiO2 - rGO 10.

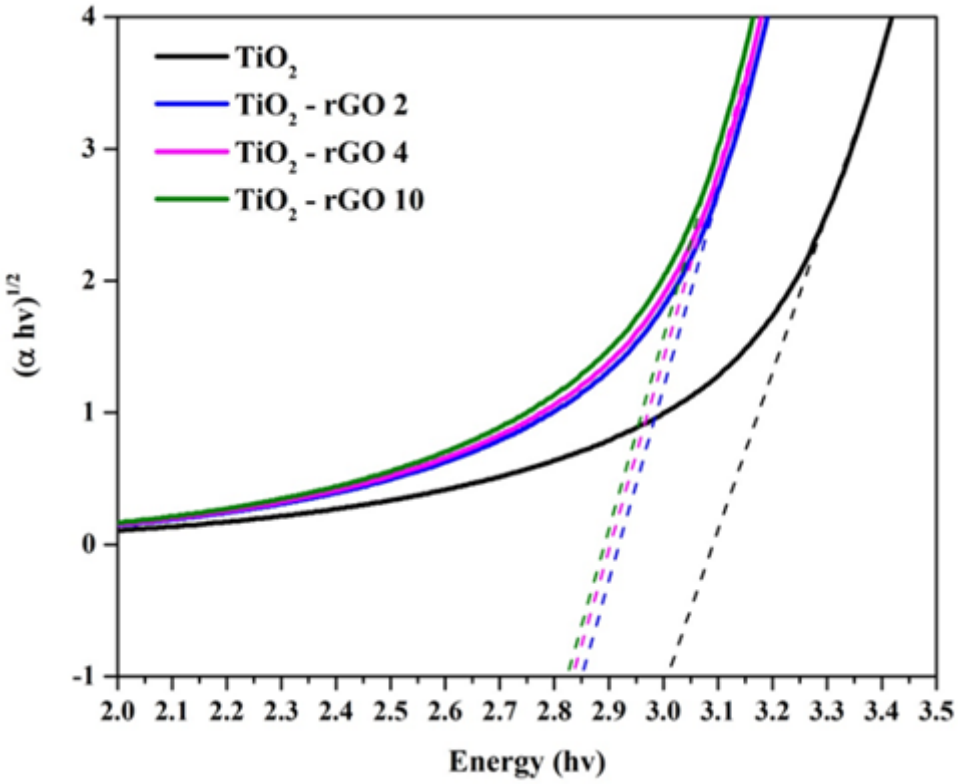

Figure 6

Band gap energy (Eg) of TiO2, TiO2-rGO 2, TiO2-rGO 4 and TiO2-rGO 10 by Tauc's Plot method.

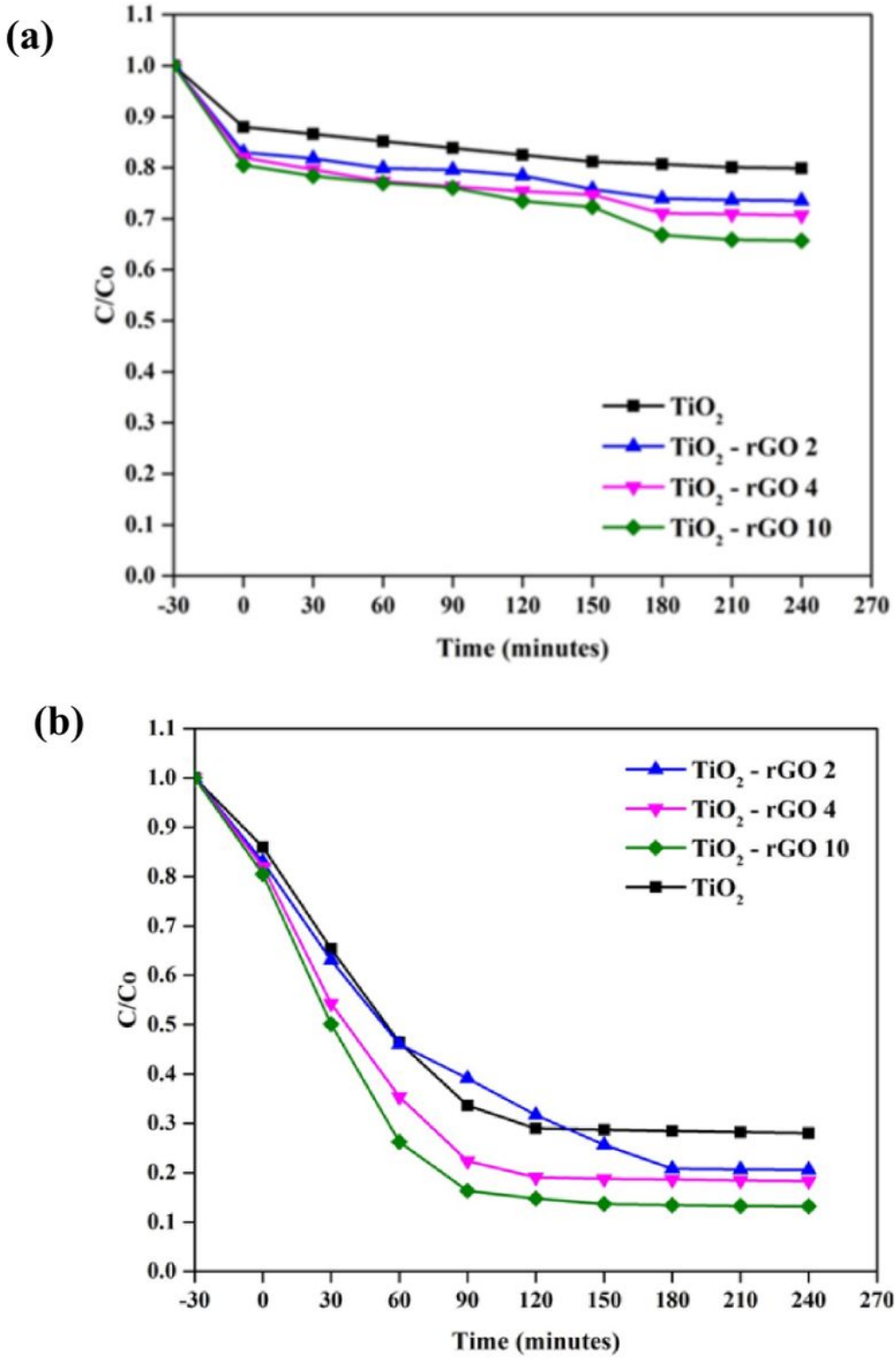

Figure 7

Result of rhodamine-B photodegradation activity of TiO2, TiO2 - rGO 2, TiO2 - rGO 4 and TiO2 - rGO 10 under (a) visible and (b) UV light irradiation.

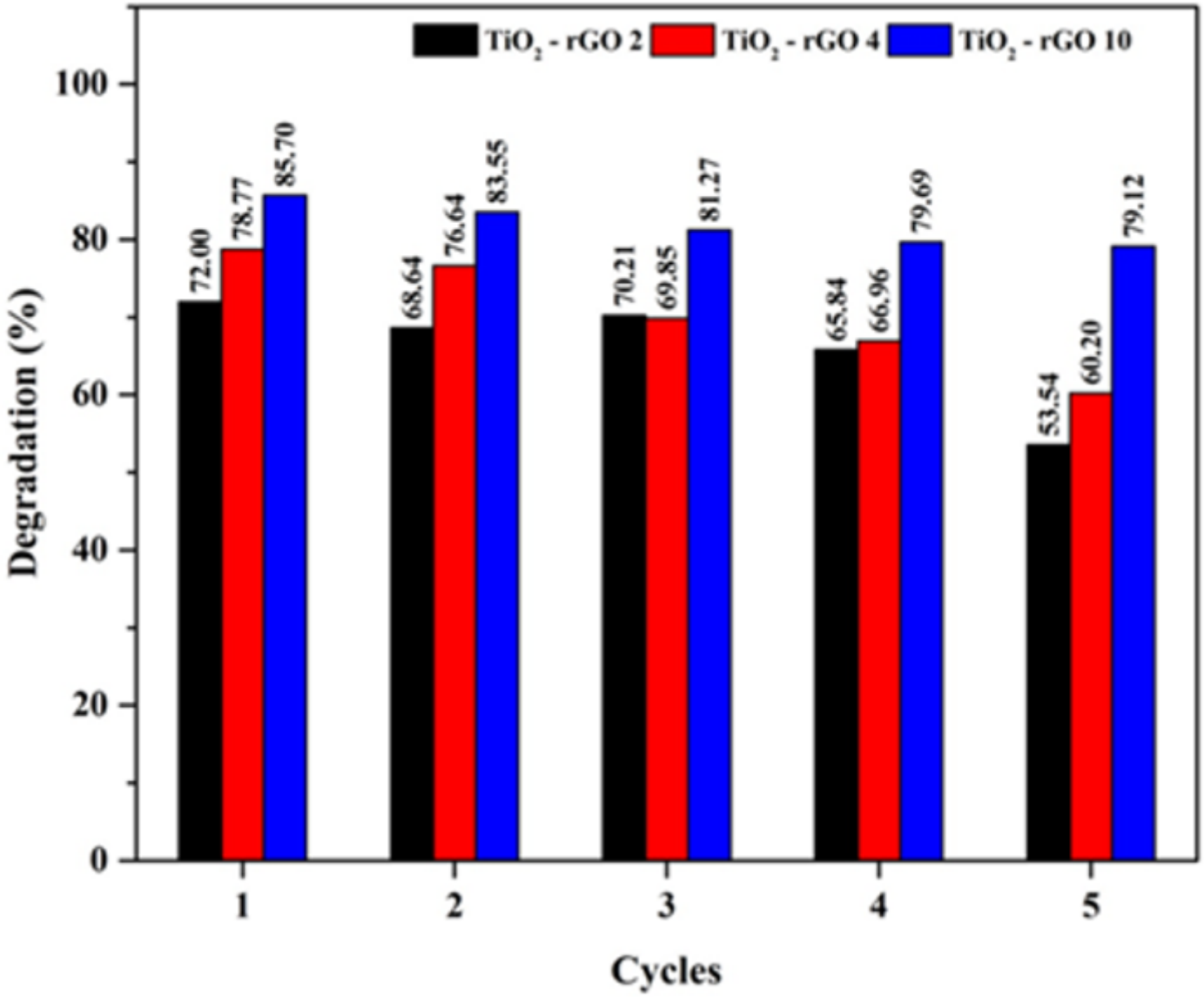

Figure 8

Photodegradation performance stability of TiO2, TiO2 - rGO 2, TiO2 - rGO 4 and TiO2 - rGO 10.

Supplementary Files

This is a list of supplementary files associated with this preprint. Click to download.

- GRAPHICALABSTRACT.png